Journal of Southeast University (English Edition) Vol. 38, No. 1, pp. 20 - 26 Mar. 2022 ISSN 1003—7985

# Detection of solar radio burst intensity based on a modified multifactor SVM algorithm

Luo Yimei[1] Zhu Xuefen[1] Lin Mengying[1] Yang Fan[1] Tu Gangyi[2]

([1]School of Instrument Science and Engineering, Southeast University, Nanjing 210096, China)

([2]School of Electronic and Information Engineering, Nanjing University of Information Science and Technology, Nanjing 210044, China)

**Abstract:** To realize the automatic detection of solar radio burst (SRB) intensity, detection based on a modified multifactor support vector machine (SVM) algorithm is proposed. First, the influence of SRB on global navigation satellite system (GNSS) signals is analyzed. Feature vectors, which can reflect the SRB intensity of stations, are also extracted. SRB intensity is classified according to the solar radio flux, and different class labels correspond to different SRB intensity types. The training samples are composed of feature vectors and their corresponding class labels. Second, training samples are input into SVM classifiers to one-against-one training to obtain the optimal classification models. Finally, the optimal classification model is synthesized into a modified multifactor SVM classifier, which is used to automatically detect the SRB intensity of new data. Experimental results indicate that for historical SRB events, the average accuracy of SRB intensity detection is greater than 90% when the solar incident angle is higher than 20°. Compared with other methods, the proposed method considers many factors with higher accuracy and does not rely on radio telescopes, thereby saving cost.

**Key words:** global navigation satellite system; solar radio burst; modified multifactor SVM algorithm; detection accuracy

**DOI:** 10.3969/j.issn.1003-7985.2022.01.004

With the wide application of global navigation satellite systems (GNSS) in modern society, the influence of solar radio burst (SRB) on GNSS signals has attracted the extensive attention of scholars. SRBs are intense radio wave emissions, usually related to solar flares[1]. Previous studies revealed that the satellite carrier-to-noise ratio ($C/N_0$) decreases, the positioning error and the geometry dilution of precision (GDOP) increase, and the navigation signals are lost to varying degrees during severe SRBs[2]. Chen et al.[3] presented that the flux density threshold of SRBs affecting GPS signals is between 4 000 and 12 000 solar flux units (SFU). Huang et al.[4] analyzed the SRB event on December 13, 2006, and found that in this event, the number of satellites locked of multiple stations was less than 4. Berdermann et al.[5], Linty et al.[6], and Sato et al.[7] analyzed the impact of the SRB event on September 6, 2017, following its effects on the ionosphere and the resulting serious problems for precise positioning and GNSS signals.

For mainly relying on manual, the traditional detection and classification of SRBs have a huge workload and low efficiency. In recent years, many methods for automatic detection and classification of SRBs have been proposed. Ma et al.[8] proposed a new SRB classification method on the basis of multimodal deep learning. Chen et al.[9] used the convolution neural network to classify the solar radio spectrum. Singh et al.[10] utilized a novel statistical method to automatically distinguish the dynamic spectrum with or without SRBs. However, this method does not classify the types of SRBs.

At present, certain methods for the automatic detection and classification of SRBs are available; most of them must be realized by radio telescope data. Given that radio telescopes are expensive and sparsely distributed, a real-time and efficient method is urgently needed to detect SRBs without utilizing radio telescopes. Yang et al.[11] proposed an intense L-band SRB detection method without the aid of a radio telescope. This method detects the valley period of the $C/N_0$ of multiple satellites and combines it with multiple stations to realize SRB detection. However, the detection feature is single and can only detect SRBs when they are severe. Huang et al.[12] gave the threshold range to define SRB intensity, providing a basis for its classification. However, they did not conduct detection.

In the present study, a method to detect SRB intensity on the basis of a modified multifactor SVM algorithm is proposed. This method detects the multiple effects of SRBs on GNSS signals, including $C/N_0$, GDOP, horizontal dilution of precision (HDOP), vertical dilution of precision (VDOP), and the number of satellites locked, to detect SRB intensity. To solve the multiple classification problems, a one-against-one method[13] is adopted.

**Received** 2021-09-23, **Revised** 2022-01-07.

**Biographies:** Luo Yimei (1997—), female, graduate; Zhu Xuefen (corresponding author), female, doctor, associate professor, zhuxuefen@seu.edu.cn.

**Foundation items:** The National Key Research and Development Plan of China (No. 2018YFB0505103), the National Natural Science Foundation of China (No. 61873064).

**Citation:** Luo Yimei, Zhu Xuefen, Lin Mengying, et al. Detection of solar radio burst intensity based on a modified multifactor SVM algorithm[J]. Journal of Southeast University (English Edition), 2022, 38(1): 20 - 26. DOI: 10.3969/j.issn.1003-7985.2022.01.004.

Every two types are combined into a binary classifier, and the classification results are obtained by voting statistics. When new data enter the classifier, it will be classified automatically.

The main advantage of this method is that it can classify SRB intensity automatically in real-time, with high efficiency. Compared with the methods proposed in previous research, the current one only uses the previous radio flux data provided by radio telescopes as the classification standard to establish the model. The subsequent classification needs the data provided by GNSS receivers, which do not rely on radio telescopes, thereby saving cost and having strong practicability. In addition, it considers many factors and has high accuracy.

## 1 Effects of SRBs on GNSS

Taking the SRB event on December 13, 2006, as an example, the effects of SRBs on GNSS signals are analyzed. At 02:14:00, an X3.4 solar X-ray flare erupted. The peak time and end time of the flare were 02:40:00 and 02:57:00, respectively, lasting for 43 min. The ground-based radio monitoring telescope recorded the whole process of the burst. Fig. 1 shows the monitoring results of L-band radio flux (represented by 1 415 MHz) provided by the Radio Solar Telescope Network (RSTN). The sampling frequency was 1 Hz. The maximum peak flux was greater than $1.1 \times 10^5$ SFU, which is nearly a thousand times higher than that during the quiet period[4].

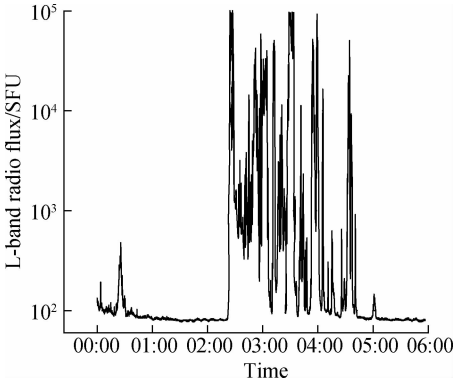


**Fig. 1** Solar radio flux at 1 415 MHz provided by RSTN on December 13, 2006

To investigate the effects of SRBs on GNSS, the NNOR station is selected as an example for analysis. Fig. 2 illustrates the variation of $C/N_0$ at GPS L1 frequency for different satellites at the NNOR station. During the SRBs, the $C/N_0$ of GPS satellites locked by the receivers of the NNOR decreased significantly, their change trend was almost identical, and the corresponding relationship with solar radio flux was obvious. The analysis reveals that the $C/N_0$ variation trend of other satellites locked at different stations is similar during SRBs.

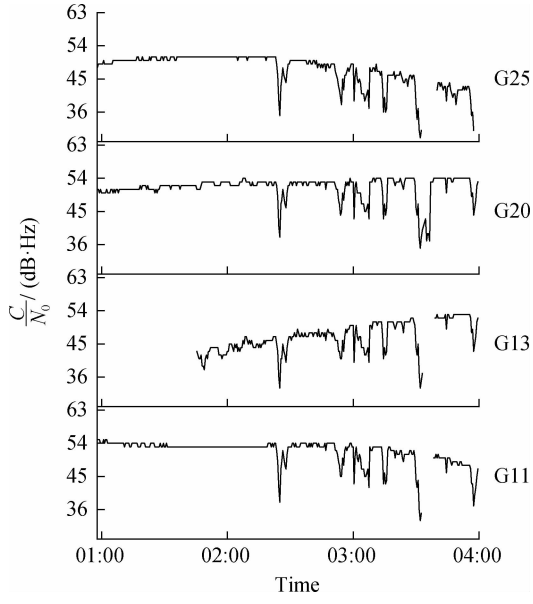


**Fig. 2** $C/N_0$ at the GPS L1 frequency for the NNOR station during the SRBs that occurred on December 13, 2006

GDOP, HDOP, and VDOP respectively represent the amplification factor of the total positioning timing error, horizontal position error, and vertical position error to the ranging error. The NNOR station is located in a plain area with flat terrain. Considering the obstructions in the signal propagation path, the elevation mask angle is set to 15° to avoid selecting invisible satellites as far as possible[14].

Fig. 3 demonstrates that during the SRB event, the GDOP, HDOP, and VDOP of NNOR increased significantly, and the maximum GDOP reached over 30.

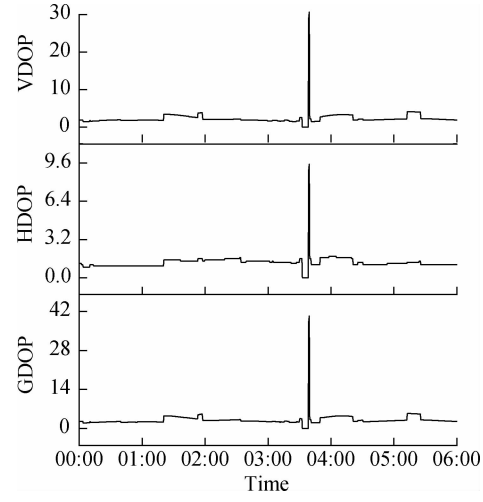


**Fig. 3** GDOP, HDOP, and VDOP variations for the NNOR station during the SRBs that occurred on December 13, 2006

Fig. 4 shows that the number of satellites locked at NNOR decreased during SRBs, which mainly occurred at 03:31:00—03:37:00.

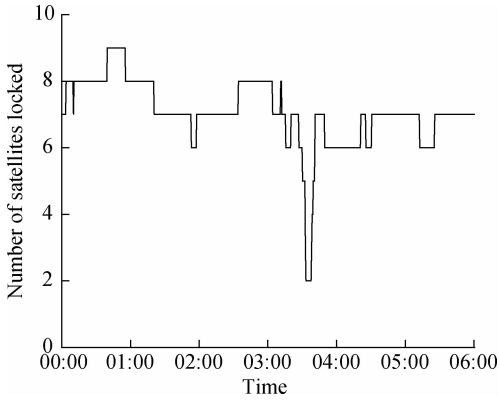


**Fig. 4** Number of satellites locked for the NNOR station during the SRBs that occurred on December 13, 2006

The analysis of several other stations shows that GDOP, HDOP, VDOP, and satellite lock numbers are also affected by SRBs. The above changes provide a basis for the selection of feature vector composition.

## 2 Methodology

### 2.1 System schema of SRB intensity detection

The system schema of the proposed method is displayed in Fig. 5, which includes training sample acquisition, model training, and SRB intensity detection.

First, $C/N_0$, GDOP, HDOP, VDOP, and the number of satellites locked are extracted. SRB intensity is labeled according to the solar radio flux. The feature vectors and labels are combined to obtain training samples.

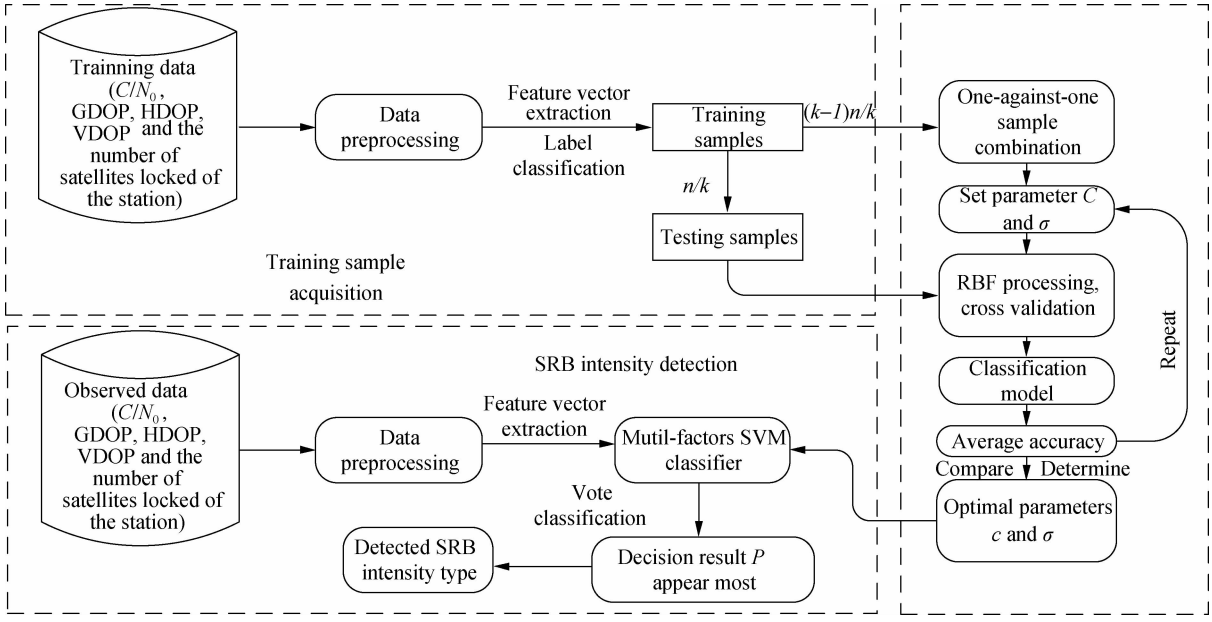


**Fig. 5** System schema of the SRB intensity detection based on a modified multifactor SVM algorithm

On the basis of the fact that SVM is a binary classifier, a one-against-one method is adopted. Samples with different labels are combined in pairs. Then, the SVM binary classification model is trained for each combination to obtain the corresponding optimal classification model. Classification models form the final modified multifactor SVM classifier.

Once the modified multifactor SVM classifier is confirmed, new feature vectors are preprocessed and input into the trained modified multifactor SVM classifier. The classifier automatically inputs the feature vectors into the trained optimal classification models. Each model outputs labels corresponding to the feature vectors. For each feature vector, the most frequent label is its corresponding intensity type by voting.

### 2.2 Training sample acquisition

Take the average of the current $C/N_0$ of each satellite captured as the $C/N_0$ of the station at the current time, recorded as $x_1$, measured in unit dB · Hz.

$$x_1 = \sum_{i=1}^{N} \frac{s_i}{N} \tag{1}$$

where $s_i$ is the $C/N_0$ of each satellite captured, $i = 1, 2, \cdots, N$. $N$ is the number of satellites captured.

The GDOP, VDOP, HDOP, and the number of satellites locked at the observation station do not have to be dealt with. Only the original data released by the International GNSS Service (IGS) are used.

The feature vectors are formed as

$$\boldsymbol{x}^{(i)} = \{x_1^{(i)}, x_2^{(i)}, x_3^{(i)}, x_4^{(i)}, x_5^{(i)}\} \qquad \boldsymbol{x}^{(i)} \in \mathbf{R}^4 \tag{2}$$

where $x_1, x_2, \cdots, x_5$ represent the $C/N_0$, GDOP, HDOP, VDOP, and the number of satellites locked, respectively.

Tab. 1 lists the SRB intensity types, radio flux thresholds, and corresponding labels[12].

$\boldsymbol{x}^{(i)}$ represents the feature vector of the sample, and $y^{(i)}$ represents the label of the sample, $i = 1, 2, \cdots, n$. $\boldsymbol{x}^{(i)}$ and

**Tab. 1** Classification of SRB intensity types

| SRB intensity type | Radio flux/SFU | $y^{(i)}$ |
|---|---|---|
| Nonoccurrence | ≤100 | 1 |
| Moderate | 100 to 10 000 | 2 |
| Severe | ≥10 000 | 3 |

$y^{(i)}$ are combined into sample point $(\boldsymbol{x}^{(i)}, y^{(i)})$.

### 2.3 Model training

One-against-many and one-against-one methods are the commonly used SVM multiple classification methods. SVM optimization problems in the one-against-many method have high computational complexity and its gaining speed slower than the one-against-one method[13]. In this study, SRBs are divided into three types, and no classification overlap occurs. Therefore, the one-against-one method for multiple classification is selected.

First, suppose that a nonlinear SVM binary classifier is constructed for the training samples with labels $u$ and $v$ ($u$, $v = 1, 2, 3$, and $u < v$). The classification model is

$$f(\boldsymbol{x}) = \boldsymbol{w}^{\mathrm{T}}\varphi(\boldsymbol{x}) + b \tag{3}$$

where $\boldsymbol{w}^{\mathrm{T}}$ is defined as the normal vector, and $b$ is defined as the intercept of the classification hyperplane. $\varphi(\boldsymbol{x})$ is a high-dimensional linear mapping.

Second, solve the following optimization problems:

$$\min_{w,b,\xi} \frac{1}{2} \| \boldsymbol{w} \|^2 + C\sum_{i=1}^{n} \xi_i \tag{4}$$

s. t.

$$y^{(i)}(\boldsymbol{w}^{\mathrm{T}}\varphi(\boldsymbol{x}^{(i)}) + b) \geqslant 1 - \xi_i,\ \xi_i \geqslant 0 \qquad i = 1, 2, \cdots, n \tag{5}$$

where $\xi_i$ is the slack variable of each sample, and $C$ is a hyperparameter.

Third, solve the Lagrangian multipliers,

$$\max \sum_{i=1}^{n} \alpha_i - \frac{1}{2}\sum_{i,j=1}^{n} \alpha_i \alpha_j y^{(i)} y^{(j)} \tag{6}$$

$$\sum_{i=1}^{n} \alpha_i y^{(i)} = 0, \quad 0 \leqslant \alpha_i \leqslant C \tag{7}$$

where $\alpha_i$, $y^{(i)}$ are the Lagrangian multipliers and data classification label, respectively, $i = 1, 2, \cdots, n$.

Furthermore,

$$w_0 = \sum_{i=1}^{n} \alpha_i y^{(i)} \varphi(\boldsymbol{x}^{(i)}) \tag{8}$$

$$b_0 = y^{(s)} - \boldsymbol{w}_0^{\mathrm{T}}\varphi(\boldsymbol{x}^{(s)}) \tag{9}$$

where $\boldsymbol{x}^{(s)}$ is the support vector, and $y^{(s)}$ is the corresponding label.

Fourth, the calculated $w$ and $b$ are substituted into the nonlinear SVM classifier model expression.

$$f(\boldsymbol{x}) = \sum_{i=1}^{n} \alpha_i y^{(i)} k(\boldsymbol{x}^{(i)}, \boldsymbol{x}) + y^{(s)} - \sum_{i=1}^{m} \alpha_i y^{(i)} k(\boldsymbol{x}^{(i)}, \boldsymbol{x}^{(s)}) \tag{10}$$

where the kernel function can be expressed as $k(\boldsymbol{x}^{(i)}, \boldsymbol{x}) = \varphi^{\mathrm{T}}(\boldsymbol{x}^{(i)})\varphi(\boldsymbol{x})$. The radial basis function (RBF) is selected as the kernel function. In the absence of prior knowledge of the training samples, as long as the parameters are selected appropriately, SVM with RBF can achieve strong learning ability. RBF is defined as

$$k(\boldsymbol{x}^{(i)}, \boldsymbol{x}) = \exp\left\{ -\frac{|\boldsymbol{x}^{(i)} - \boldsymbol{x}|^2}{2\sigma^2} \right\} \tag{11}$$

where $\sigma$ is the kernel parameter.

Select $k$-fold cross validation, which enables the model to encounter various data through multiple division and training to improve its generalization ability.

Select the Gaussian nonlinear SVM classifier model and set parameters $C$, $1/(2\sigma^2)$. After training, the average accuracy of these parameter settings is obtained.

Change the value of parameters:

$$C = 2^m \qquad m = -5, -4, \cdots, 10$$

$$\frac{1}{2\sigma^2} = 2^n \qquad n = -5, -4, \cdots, 10$$

By comparing the average accuracy of all parameter settings, parameters $C$ and $\sigma$ with the maximum accuracy are found as the optimal parameters. The trained model under the optimal parameter setting is the optimal classification model. Three optimal classification models form the final modified multifactor SVM classifier.

### 2.4 SRB intensity detection

The feature vectors of the newly observed data are expressed as $\boldsymbol{X} = \{\boldsymbol{x}^{(1)}, \boldsymbol{x}^{(2)}, \cdots, \boldsymbol{x}^{(N)}\}$. $N$ is the total number of samples to be detected.

Input $\boldsymbol{X}$ into the modified multifactor SVM classifier, and the voting strategy is adopted. For each feature vector $\boldsymbol{x}^{(i)}$, if label $P$ ($P = 1, 2, 3$) outputs after an optimal classification model of the modified multifactor SVM classifier completes the work, the number of label $P$ is added by one. The label that appears the most is the detected type of SRB intensity at that time at the station.

## 3 Results and Discussion

### 3.1 Single station detection process

Take KUNM as an example. To train the modified multifactor SVM classifier, the data of KUNM at 01:30:00—03:59:30 on December 13, 2006, are selected, including $C/N_0$, GDOP, HDOP, VDOP, and locked satellites. After data preprocessing and label allocation, the training samples of KUNM are obtained from the IGS Data Center of Wuhan University. The sampling interval is 30 s, and each station has 300 times in total. Tab. 2 lists five relatively representative sample points.

**Tab. 2** Sample points corresponding to different times of the KUNM station

| Time | Sample point |
|---|---|
| 02:00:00 | (46.444 44, 1.8, 0.9, 1.4, 8,1) |
| 02:59:30 | (46.656 25, 2.2, 1, 1.6, 7, 2) |
| 03:31:30 | (42.000 00, 16.7, 5.5, 11.7, 4,3) |
| 03:36:00 | (41.416 67, /, /, /, 3, 3) |
| 03:52:00 | (47.437 50, 2.1, 1.2, 1.5, 7, 1) |

Note: / represents data that cannot be obtained.

The training samples are input into the SVM classification learner, cross validation is conducted, and the $k$-fold number is set to $k=5$. Through training, three classification models under the optimal parameter setting are obtained. When $C=8$, $1/(2\sigma^2)=1$, the classifiers of Types 1 and 2 have the highest average accuracy of 96.8%. When $C=2$, $1/(2\sigma^2)=0.5$, the average accuracy of the optimal classifiers of Types 1 and 3 is 98.8%. When $C=8$, $1/(2\sigma^2)=1$, the average accuracy of the optimal classifiers of Types 2 and 3 is 94.0%.

The confusion matrix and ROC curve of optimal classification models are shown in Fig. 6. Each column of the confusion matrix represents the prediction type, whereas each row represents the actual type. As displayed on the left in Figs. 6(a) to (c), 94% with Type 1 and 99% of the sample points with Type 2 SRB intensity are detected correctly.

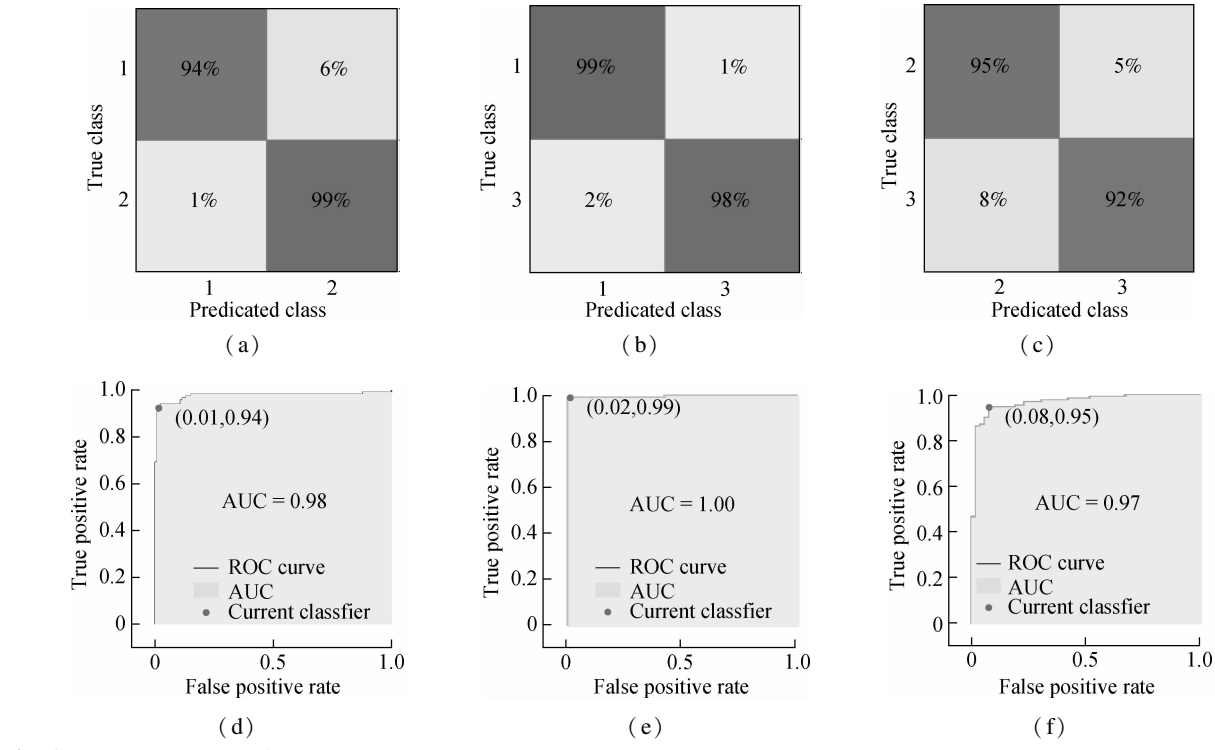


**Fig. 6** Detection results of SRB intensity in KUNM. (a) Confusion matrix of Types 1&2; (b) Confusion matrix of Types 1&3; (c) Confusion matrix of Types 2&3; (d) ROC curve of Types 1&2; (e) ROC curve of Types 1&3; (f) ROC curve of Types 2&3

The ROC curve reflects the relationship between sensitivity and specificity. The area under the curve (AUC) is used to indicate the detection accuracy. The higher the AUC value (the maximum value is 1) and the closer the curve is to the upper left corner, the higher the prediction accuracy. According to Figs. 6(d) to (f), each model has high detection accuracy.

### 3.2 Detection results of multiple stations

To expand data coverage, two additional typical SRBs are analyzed, that is, SRBs on September 24, 2011, and September 6, 2017.

For each event, four stations are selected. Tabs. 3 to 5 list the station detail and the average accuracy corresponding to the optimal model.

As can be seen from Tabs. 3 to 5, for three different SRB events, the average accuracy of any classifier at different stations is between 91% and 100%.

### 3.3 Influence of feature vector composition on average accuracy

To simplify the data preprocessing, this study tests whether a higher average accuracy can still be obtained when there were fewer combined feature vectors during the SRBs on December 13, 2006. The $C/N_0$, GDOP, HDOP, VDOP, and the number of satellites locked of the station are removed.

As illustrated in Fig. 7, the height of each column is the difference between the average accuracy of the original vectors and that of the vectors with a feature removed. If it is a positive number, then the average accuracy decreases. On the contrary, the average accuracy increases.

**Tab. 3** Average accuracy of different stations during the SRBs on December 13, 2006 (detection period 00:00—10:00)

| Station ID | Latitude and longitude | Solar incidence angle/(°) | Type | Average accuracy/% |
|---|---|---|---|---|
| TWTF | 121°E, 25°N | 42.5 | 1&2 | 93.5 |
| | | | 1&3 | 96.4 |
| | | | 2&3 | 91.3 |
| KUNM | 103°E, 25°N | 35.9 | 1&2 | 91.6 |
| | | | 1&3 | 97.0 |
| | | | 2&3 | 90.4 |
| XIAN | 109°E, 34°N | 29.3 | 1&2 | 93.2 |
| | | | 1&3 | 97.8 |
| | | | 2&3 | 93.8 |
| NNOR | 116°E, 31°S | 77.1 | 1&2 | 91.8 |
| | | | 1&3 | 97.6 |
| | | | 2&3 | 91.0 |

**Tab. 4** Average accuracy of different stations during the SRBs on September 24, 2011 (detection period 10:26—21:50)

| Station ID | Latitude and longitude | Solar incidence angle/(°) | Type | Average accuracy/% |
|---|---|---|---|---|
| RABT | 7°W, 33°N | 56.2 | 1&2 | 99.2 |
| | | | 1&3 | 100 |
| | | | 2&3 | 99.7 |
| MAS1 | 16°W, 27°N | 63.0 | 1&2 | 99.2 |
| | | | 1&3 | 100 |
| | | | 2&3 | 99.7 |
| CHPI | 45°W, 22°S | 53.4 | 1&2 | 98.7 |
| | | | 1&3 | 100 |
| | | | 2&3 | 99.8 |
| AREQ | 72°W, 16°S | 31.6 | 1&2 | 99.3 |
| | | | 1&3 | 100 |
| | | | 2&3 | 99.4 |

**Tab. 5** Average accuracy of different stations during the SRBs on September 6, 2017 (detection period 05:00—15:21)

| Station ID | Latitude and longitude | Solar incidence angle/(°) | Type | Average accuracy/% |
|---|---|---|---|---|
| VILL | 4°W, 40°N | 49.8 | 1&2 | 97.2 |
| | | | 1&3 | 99.9 |
| | | | 2&3 | 98.8 |
| SFER | 7°W, 36°N | 53.4 | 1&2 | 97.2 |
| | | | 1&3 | 99.9 |
| | | | 2&3 | 98.2 |
| MBAR | 30°E, 0°N | 60.0 | 1&2 | 94.6 |
| | | | 1&3 | 99.3 |
| | | | 2&3 | 95.5 |
| HARB | 27°E,25°S | 53.9 | 1&2 | 94.1 |
| | | | 1&3 | 99.9 |
| | | | 2&3 | 97.0 |

When the influence of $C/N_0$ or the number of satellites locked is removed, the average accuracy decreases mostly, with a maximum decrease of 20.3%. The average accuracy loss is less than any classifier with one of GDOP, HDOP, and VDOP removed at different stations and can still reach 85%. In sum, when the average accuracy requirement is not strict, one of the GDOP, HDOP, and VDOP can be removed from the feature vectors.

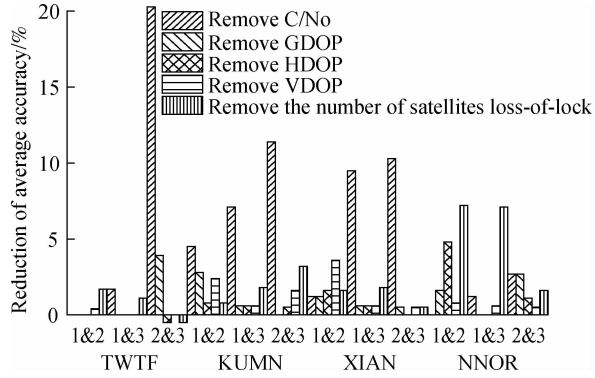


**Fig. 7** Difference in average accuracy between original vectors and vectors with any feature removed

Fig. 8 demonstrates that the average accuracy of any model is reduced if two of the three less influential feature vectors are removed at the same time.

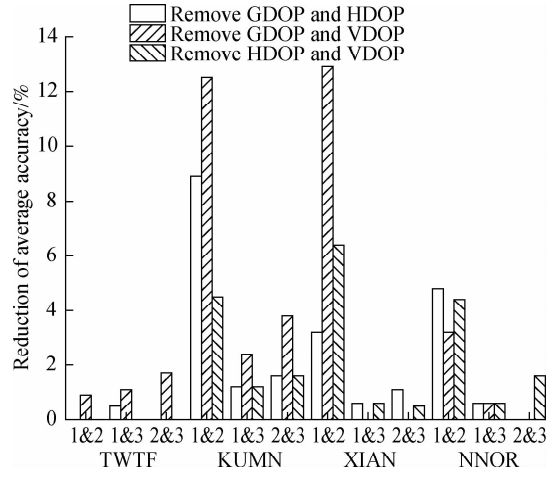


**Fig. 8** Difference in average accuracy between the original vectors and vectors with two features removed

## 4 Conclusions

1) SRB intensity detection based on a modified multifactor SVM algorithm can process a large amount of data simultaneously and detect SRB intensity in multiple stations at the same time.

2) The proposed method not only improves detection reliability, efficiency, and accuracy by considering various factors but also saves cost, as it does not require the use of radio telescopes. Thus, it is expected to be a useful tool in the normal operation of the satellite navigation system.

3) Using the original feature vectors in this study, the average accuracy can reach more than 90%. If the accuracy requirement is not strict, then one of GDOP, HDOP, and VDOP can be removed from the feature vectors. However, two features cannot be removed at the same time, as it can lead to inaccurate detection results.

## References


[1] Zheng Z. *Solar radio spectrum image classification based on deep learning* [D]. Dalian: Dalian University of Technology, 2019. (in Chinese)

[2] Dong L. *Research on evaluation and early warning scheme of solar radio burst jamming communication system* [D]. Kunming: Yunnan University, 2016. (in Chinese)

[3] Chen Z, Gao Y, Liu Z. Evaluation of solar radio bursts' effect on GPS receiver signal tracking within International GPS service network [J]. *Radio Science*, 2005, **40**(3): 1-11. DOI:10.1029/2004RS003066.

[4] Huang W G, Arer C, Shen H, et al. Impact of intense L-band solar radio burst on GNSS performance and positioning accuracy[J]. *Chinese Journal of Radio Science*, 2018, **33**(1): 1-7. DOI: 10.13443/j.cjors.2017062202. (in Chinese)

[5] Berdermann J, Kriegel M, Banyś D, et al. Ionospheric response to the X9.3 flare on 6 September 2017 and its implication for navigation services over Europe [J]. *Space Weather*, 2018, **16**(10): 1604-1615. DOI:10.1029/2018sw001933.

[6] Linty N, Minetto A, Dovis F, et al. Effects of phase scintillation on the GNSS positioning error during the September 2017 storm at svalbard[J]. *Space Weather*, 2018, **16**(9): 1317-1329. DOI: 10.1029/2018sw001940.

[7] Sato H, Jakowski N, Berdermann J, et al. Solar radio burst events on 6 September 2017 and its impact on GNSS signal frequencies[J]. *Space Weather*, 2019, **17**(6): 816-826. DOI:10.1029/2019sw002198.

[8] Ma L, Chen Z, Xu L, et al. Multimodal deep learning for solar radio burst classification[J]. *Pattern Recognition*, 2017, **61**: 573-582. DOI: 10.1016/j.patcog.2016.04.013.

[9] Chen S S, Xu L, Ma L, et al. Convolutional neural network for classification of solar radio spectrum[C]//2017 *IEEE International Conference on Multimedia & Expo Workshops*. Hong Kong, China, 2017: 198-201. DOI: 10.1109/ICMEW.2017.8026227.

[10] Singh D, Sasikumar Raja K, Subramanian P, et al. Automated detection of solar radio bursts using a statistical method[J]. *Solar Physics*, 2019, **294**(8): 1-14. DOI:10.1007/s11207-019-1500-0.

[11] Yang F, Zhu X F, Chen X Y, et al. Intense L-band solar radio bursts detection based on GNSS carrier-to-noise ratio decrease over multi-satellite and multi-station[J]. *Sensors*, 2021, **21**(4): 1405. DOI:10.3390/s21041405.

[12] Huang W G, Aa E C, Shen H, et al. Statistical study of GNSS L-band solar radio bursts [J]. *GPS Solutions*, 2018, **22**(4): 1-9. DOI:10.1007/s10291-018-0780-4.

[13] Xue N J. Comparison of multi-class support vector machines[J]. *Computer Engineering and Design*, 2011, **32**(5): 1792-1795. DOI:10.16208/j.issn1000-7024.2011.05.080. (in Chinese)

[14] Niu Q, Li L N. Influence of satellite elevation mask measured by GPS long baseline on positioning accuracy [J]. *Zhejiang Agricultural Science*, 2016, **57**(8): 1316-1318. DOI: 10.16178/j.issn.0528-9017.20160850. (in Chinese)


# 基于改进的多因素 SVM 算法的太阳射电暴强度检测


罗铱镅[1] 祝雪芬[1] 林梦颖[1] 杨 帆[1] 涂刚毅[2]

([1] 东南大学仪器科学与工程学院,南京 210096)

([2] 南京信息工程大学电子与信息工程学院,南京 210044)



**摘要:** 为实现对太阳射电暴(SRBs)强度的自动检测,提出了一种基于改进的多因素支持向量机(SVM)的 SRBs 强度检测方法. 首先,分析 SRBs 对全球导航卫星系统(GNSS)信号的影响,提取能够反映接收站点 SRBs 强度的特征向量. 根据太阳射电流量对 SRBs 强度进行分类标签,不同标签对应不同 SRBs 强度类型,训练样本由特征向量及其标签组成. 其次,将具有不同标签的训练样本输入 SVM 分类器,进行一对一训练,得到最优分类模型. 最后,将最优分类模型合成为改进的多因素 SVM 分类器,用于自动识别更新后的 SRBs 样本. 实验结果表明,对于历史 SRBs 事件,当太阳入射角大于 20°时,SRBs 强度检测的平均准确率在 90% 以上. 该算法综合考虑了多种因素,可进行 SRBs 强度的自动检测,与其他方法相比,该方法不依赖射电望远镜,节约了成本且检测精度更高.



**关键词:** 全球导航卫星系统;太阳射电爆发;改进的多因素支持向量机;检测精度

**中图分类号:** TN967.1